

# Insights into Intramolecular Trp and His Side-Chain Orientation and Stereospecific $\pi$ Interactions Surrounding Metal Centers: An Investigation Using Protein Metal-Site Mimicry in Solution

Chi Ming Yang\* and Jie Zhang<sup>[a]</sup>

**Abstract:** Metal-binding scaffolds incorporating a Trp/His-paired epitope are instrumental in giving novel insights into the physicochemical basis of functional and mechanistic versatility conferred by the Trp–His interplay at a metal site. Herein, by coupling bio-metal site mimicry and  $^1\text{H}$  and  $^{13}\text{C}$  NMR spectroscopy experiments, modular constructs EDTA-(L-Trp, L-His) (EWH; EDTA = ethylenediamino tetraacetic acid) and DTPA-(L-Trp, L-His) (DWH; DTPA = diethylenetriamino pentaacetic acid) were employed to dissect the static and transient physicochemical properties of hydrophobic/hydrophilic aromatic interactive modes surrounding biometal centers. The binding feature and identities of the stoichiometric metal-bound complexes in solution were investigated by using  $^1\text{H}$  and  $^{13}\text{C}$  NMR spectroscopy, which facilitated a cross-validation of the carboxylate, amide oxygen, and tertiary amino groups as the pri-

mary ligands and indole as the secondary ligand, with the imidazole (Im) N3 nitrogen being weakly bound to metals such as  $\text{Ca}^{2+}$  owing to a multivalency effect. Surrounding the metal centers, the stereospecific orientation of aromatic rings in the diastereoisomerism is interpreted with the  $\text{Ca}^{2+}$ –EWH complex. With respect to perturbed Trp side-chain rotamer heterogeneity, drastically restricted Trp side-chain flexibility and thus a dynamically constrained rotamer interconversion due to  $\pi$  interactions is evident from the site-selective  $^{13}\text{C}$  NMR spectroscopic signal broadening of the Trp indolyl C3 atom. Furthermore, effects of Trp side-chain fluctuation on indole/Im orientation were the subject of a 2D

NMR spectroscopy study by using the  $\text{Ca}^{2+}$ -bound state; a C–H2(indolyl)/C–H5(Im<sup>+</sup>) connectivity observed in the NOESY spectra captured direct evidence that the N–H1 of the  $\text{Ca}^{2+}$ –Im<sup>+</sup> unit interacted with the pyrrole ring of the indole unit in  $\text{Ca}^{2+}$ -bound EWH but not in DWH, which is assignable to a moderately static, anomalous, T-shaped, interplanar  $\pi^+ - \pi$  stacking alignment. Nevertheless, a comparative  $^{13}\text{C}$  NMR spectroscopy study of the two homologous scaffolds revealed that the overall response of the indole unit arises predominantly from global attractions between the indole ring and the entire positively charged first coordination sphere. The study thus demonstrates the coordination-sphere/geometry dependence of the Trp/His side-chain interplay, and established that  $\pi$  interactions allow  $^{13}\text{C}$  NMR spectroscopy to offer a new window for investigating Trp rotamer heterogeneity near metal-binding centers.

**Keywords:** amino acids • conformation analysis • NMR spectroscopy • noncovalent interactions • pi interactions

## Introduction

Our understanding of the importance of side-chain-specific interactions in proteins is being significantly advanced through investigations of the aromatic interaction interface,

which plays crucial roles in protein structure and functions.<sup>[1,2]</sup> Aromatic side-chain interactions also serve as mediators or form a complementary interface in protein–protein and protein–ligand interactions.<sup>[1,2]</sup> With respect to metalloproteins, active-site aromatic interactions significantly tune the metal-site reactivity due to subtle structural or electronic alterations.<sup>[3]</sup> For example,  $\pi$  stacking of a second-coordination-sphere Trp (W) residue in metalloenzymes has profound effects on active-site geometric and electronic structures and functions.<sup>[4]</sup> However, aromatic interactions around metal sites are incompletely understood. As more discrete roles for second-sphere aromatic residues in metalloprotein active sites become apparent (of particular inter-

[a] Prof. Dr. C. M. Yang, J. Zhang  
Neurochemistry & Biophysical Organic Chemistry  
College of Chemistry, Nankai University  
Tianjin 300071 (China)  
Fax: (+86) 22-2350-8074  
E-mail: yangchm@nankai.edu.cn

Supporting information for this article is available on the WWW under <http://dx.doi.org/10.1002/chem.200903149>.

est currently are the cation- $\pi$  and  $\pi$ - $\pi$  interactions associated with second-sphere aromatic ligands),<sup>[4,5a-g]</sup> so has the need for well-characterized biomimetic structural/mechanistic models for in-depth investigations.

Although it is realized that Trp/His side chains play numerous functional roles in metalloprotein active sites, the physicochemical basis of such functional roles have remained poorly understood. The indole and imidazole moieties are structurally and functionally among the most versatile side-chain groups present in proteins. Indeed, uniquely paired Trp/His- or Trp/His-rich motifs embedded in proteins are pivotal to a variety of biological functions.<sup>[6-8]</sup> The intrinsically multifunctional significance of a Trp/His pair is often a major constituent of structural/mechanistic hotspots implicated in the functions of diverse important proteins including Mn- and Fe-superoxide dismutase,<sup>[5h-j,6a]</sup> galactose oxidase,<sup>[6b]</sup> ion channels,<sup>[6c]</sup> interleukins,<sup>[6d]</sup> and human Trp dioxygenase,<sup>[6e]</sup> and notably, in an elusive function and etiological role of prion octarepeats (Pro-His-Gly-Gly-Gly-Trp-Gly-Gln).<sup>[7]</sup> It is, therefore, evident that the metal-site Trp/His pair plays multifaceted roles in proteins, and understanding these roles requires a detailed appreciation of how the chemistry of Trp/His is modulated by the metal coordination environment. In this regard, the hydrophobic/hydrophilic pairwise aromatic interactions of Trp/His, which are important contributory factors to protein structure and function, have been the subject of much interest in chemistry and biochemistry.<sup>[6-8]</sup>

Metal-binding specificity is not only fundamental to metal sites in metalloproteins,<sup>[9]</sup> but also a viable factor in controlling protein-ligand interactions,<sup>[10a-d]</sup> protein self-assembly,<sup>[10e]</sup> and aggregation.<sup>[7]</sup> The design of metalloproteins and metal-coordinating motifs incorporating isolated functional segments by using non-natural metal ligands can provide insights into the structure and function of natural metalloproteins and enzymes; this could potentially lead to functional metalloprotein mimics and spectroscopic probes for studying protein interactions.<sup>[10b,e,11]</sup>

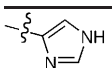
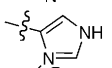
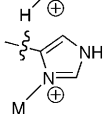
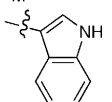
In metalloproteins, although the Im side chain is the most common metal-binding residue, the electron-rich indole ring of Trp is the strongest  $\pi$ -electron donor and a very important component of the aromatic nucleus residing within the hydrophobic cluster shells outside the first coordination sphere of metal centers in metalloproteins.<sup>[3,4,6a,b,7,8a]</sup> The outer-sphere association of a Trp indole side chain together with the prevalence of Trp/His pairs in a wide range of structurally defined metalloproteins suggest that it might play even more hitherto unrecognized roles in protein function (particularly in prion proteins) beyond those that have been recently recognized,<sup>[7]</sup> such as accelerating charge transfer and electron transfer by multistep electron tunneling<sup>[12a-c]</sup> or electron hopping,<sup>[12d]</sup> facilitating hydrogen atom tunneling,<sup>[6f]</sup> and stabilizing adjacent one-electron-oxidized amino acid radicals.<sup>[3,4]</sup>

Nevertheless, the elucidation of indole/imidazole contacts is confounded by the fact that this discrete aromatic pair might engage in a range of contacts.<sup>[8]</sup> The difficulties associ-

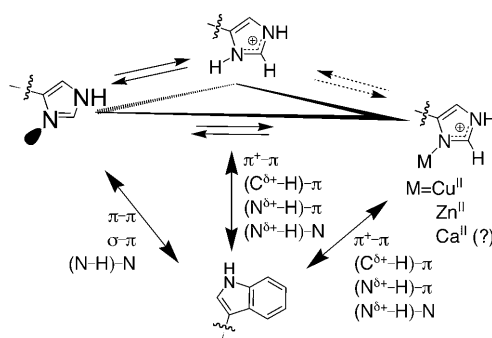
ated with experimental studies into these contacts arise from the different types of alignment between the two aromatic rings, including a competition between the T-shaped (edge-to-face) orthogonal arrangement preferred in nonpolar solvents and the  $\pi$ - $\pi$  parallel (face-to-face) stacking favored in water.<sup>[8]</sup> Furthermore, the imidazole side chain has a  $pK_a$  of  $\approx 6.0$ , and its protonation produces an imidazolium unit, which forms cation- $\pi$  and/or hydrogen bonds with Trp.<sup>[13,14]</sup>

Moreover, metal-bound imidazolium units display significantly different properties toward indole rings (Table 1).

Table 1. The basic chemical properties of aromatic species around Trp/His-containing metal-binding centers.

	Electronic character	H <sup>+</sup>	Hydrogen bonding
	strong $\sigma$ donor weak $\pi$ donor	acceptor	donor/acceptor
	$\pi$ acceptor	donor	donor
	$\pi$ acceptor	donor	donor
	strong $\pi$ donor	weak donor	donor

Consequently, there can be three types of aromatic interactive pairs incurring from a Trp/His-containing metal-binding site, possibly featuring multiple, co-existing noncovalent interactions (Scheme 1). In this regard, it can be postulated



Scheme 1. Three types of aromatic interactive pairs incurred from Trp/His-containing metal-binding centers, possibly featuring multiple coexisting noncovalent interactions.

that the unique functional and mechanistic versatility of metal-site Trp/His side-chain interactions are achieved through the control of the spatial and/or temporal distribution of noncovalent interactive feature.<sup>[6-7]</sup>

$\pi$  Interactions based on the cooperative alignment of multiple distinct aromatic side chains play an intriguing role in

the specific metal recognition and function of proteins,<sup>[7h,i]</sup> and can also serve as the mechanistic determinants of epitopes in a number of viral infection/immune response interactive events.<sup>[15]</sup> The His/Trp pair placed at *i* and *i*+4 positions on  $\alpha$  helices revealed that, depending on the protonation state of His, cation- $\pi$  or  $\pi$ - $\pi$  His/Trp interactions can act as a stabilizing factor.<sup>[13,14]</sup> However, this notion involves several unresolved ambiguities linked to conceptions of 1) whether a protonated imidazole ring interacts with an indole ring through a cationic nitrogen atom of imidazolium unit or by using the whole delocalized imidazolium ring, 2) how Trp side-chain fluctuations affect Im/indole pairwise electrostatic interactions because Trp rotamers have different electrostatic environments,<sup>[2]</sup> and 3) a likely stacking mode between the Trp/His aromatic rings depending on its microenvironment.<sup>[18]</sup> Resolution of these questions requires a structurally more defined system coupled with appropriate instrumentation for investigation.

To this end, we employed a modular biomimetic construction approach to examine the static and transient physicochemical properties inherent in the stereospecific  $\pi$  interaction of bioaromatic rings in solution. Mononuclear metal-binding site mimics incorporating Trp and His, which are both multivalent ligands for metal ions, allowed us to explore the intricate properties of dynamic aromatic interactions experienced by an extended coordination network, with special attention to Trp side-chain rotamer conformation, Im/indole alignment, and interaction modes.

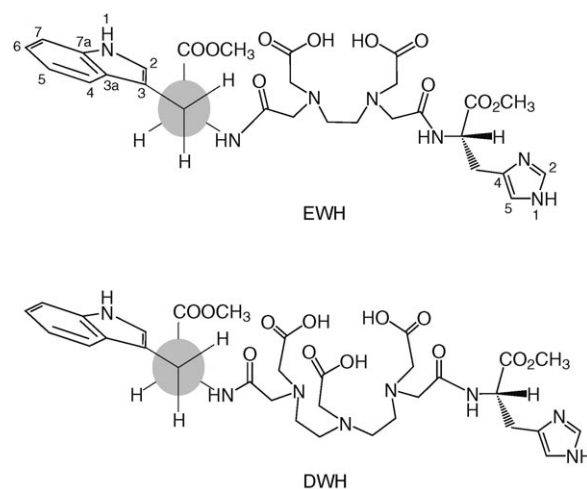
Herein, we demonstrate the context-dependent nature of the intramolecular indole/Im interplanar orientation. Side-chain rotamer oscillations affected by side-chain cation- $\pi$  interactions and possible imidazolium/indole interplanar orientation are extracted from the metal-motif mimics for in-depth inspection. In addition, we show that <sup>13</sup>C NMR spectroscopic study of Trp-containing molecules that engage in cation- $\pi$  interactions offers a different means of obtaining unambiguous evidence for Trp rotamer behavior and represents a new indirect tool for revealing the rotamer conformation change in the Trp side chain. This study should, therefore, contribute to the understanding of Trp side-chain rotamer heterogeneity associated with metal-binding sites in proteins.

## Results and Discussion

### Metal-binding-site mimicry featuring Trp/His side chains

**Incorporation of a rotamer Trp residue into metal-coordinating constructs:** Chemical modification of multidentate aminocarboxylate ligands have now emerged as a viable platform for noncovalent binding studies<sup>[16,17a,b]</sup> and engineering functional ligands.<sup>[17c-f]</sup> In this context, we employed ethylenediamino tetraacetic acid (EDTA) and diethylenetriamino pentaacetic acid (DTPA) as chelator platforms for the presentation of the indole-imidazole interactions surrounding metal centers. We prepared hetero-bifunctionally

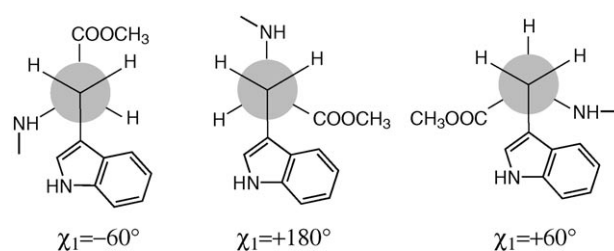
modified chelators encompassing a Trp/His motif, EDTA-(L-Trp methyl ester, L-His methyl ester) (EWH) and DTPA-(L-Trp methyl ester, L-His methyl ester) (DWH) by using a three-component coupling reaction (see Scheme 2).<sup>[18]</sup> The



Scheme 2. Chemical structure of hetero-bifunctionally modified EDTA-bisamide and DTPA-bisamide ligands, featuring a His side chain and a rotameric Trp side chain.

basic chemical structure of the biomimetic constructs consists modularly of an EDTA-bisamide and a DTPA-bisamide, each of the individual bisamide bearing two different types of peptidyl functionalities incorporating a Trp/His pair. Both the constructs were shown to be capable of mononuclear biometal binding. Each Trp/His-containing bisamide features amide oxygen(s), a His imidazole ring, and bi- and tridentate aminocarboxylate groups, all of which are important ligands in the first coordination sphere of biometals, thereby providing Trp and His peptidyl aromatic side chains that mimic protein-metal binding sites.

In general, amino acids have side-chain rotamer preferences that depend on the backbone and side chain groups (Schemes 2 and 3).<sup>[2,19]</sup> Due to the large size of the indole aromatic ring, Trp rotamers are susceptible to different electrostatic environments,<sup>[2]</sup> and the Trp rotamer conformation is significant to the structure and function of the protein. Indeed, certain higher-energy rotameric states due to local steric and pairwise electrostatic interactions have a potential



Scheme 3. Newman projections of the three  $\chi_1$  rotamer structures along the  $C_\alpha$ - $C_\beta$  bond of Trp. Each  $\chi_1$  rotamer has a major  $\chi_2$  rotamer.

in regulating protein function.<sup>[2]</sup> Therefore, it is anticipated that the above-described scaffolds might provide a novel vehicle for the spectroscopic observation of rotamer conversion as it is perturbed by metal-binding-induced electrostatic interactions.<sup>[20]</sup>

Rotamers are generally defined as low-energy side-chain conformations, and the backbone conformation changes the occurrence of rotamers. Rotation about the  $C_\alpha$ – $C_\beta$  bond of Trp gives rise to the three  $\chi_1$  rotamer forms ( $t$ ,  $g^+$ ,  $g^-$ ) depicted as the Newman projections in Scheme 3, in which  $\chi_1$  is defined by the internal rotation around bond  $C_\alpha$ – $C_\beta$  and  $\chi_2$  by the bond  $C_\beta$ – $C_\gamma$ . There are six low-energy rotamer conformations that are defined by the torsional angles about the  $C_\alpha$ – $C_\beta$  ( $\chi_1 = \pm 60$  and  $180^\circ$ ) and  $C_\beta$ – $C_\gamma$  ( $\chi_2 = \pm 90^\circ$ ) bonds.<sup>[19,20]</sup> Reduced Trp rotamer flexibility is observable on enzyme–substrate binding,<sup>[2a]</sup> and recently the role of the side-chain fluctuations in pairwise electrostatic interactions has received particular attention in protein design and structural mimicry of a G-protein-coupled receptor.<sup>[2b,c]</sup>

In our structural/mechanistic models, independent variables incorporated into the metal-binding site mimic include various combination of aminocarboxylate groups, aromatic side-chain groups, negative charge (Scheme 2), and the length and flexibility of the scaffolds, which might affect side-chain rotameric states and side-chain interactions. Most importantly, the widely considered Trp/His peptidyl aromatic pair, in conjunction with the charge of divalent metal complexes, is integrated into the designed architecture.

The scaffolds comprised of a His/Trp pair present paradigmatic models for the investigation of Trp side-chain rotamer fluctuation under intramolecular cation– $\pi$  interactions in the environment of peptidyl metal-binding sites. In the design, we took the advantage of multivalency effect of the multi-aminocarboxylate ligand to enhance the metal-ion affinity of an Im ring, and we exploited such enhanced metal-binding ability of Im to fix the  $\text{Im}^+$  state, which is placed at variable distance with respect to an indole ring. By coupling  $^1\text{H}$  and  $^{13}\text{C}$  NMR spectroscopy experiments and Molecular Mechanics Force Field (MMFF) calculations, we characterized the metal-binding properties of EWH and DWH, with special attention to the electronic adaptation of the first and secondary coordination spheres of metal ions. Consequently, the scaffolds permit a manipulation of spatial orientation of aromatic side chains to alter the sterics encompassing metal centers. Divalent main-group and late first-row transition-metal ions were selected for a demonstration of the metal-motif design tactic in illuminating characteristic noncovalent interaction within the second coordination sphere.

### A solution-phase NMR spectroscopy study

**A comparative study of Trp side-chain fluctuations by using  $^1\text{H}$  and  $^{13}\text{C}$  NMR spectroscopy:** Solution-phase NMR spectroscopy has become a powerful technology for the investigation of site-specific interactions and biomolecular dynamics.<sup>[21]</sup> Chemical shifts depend on the electronic environment of nuclei, and thus hold valuable information about the

local structure. Extraction of semiquantitative structural information from chemical shift data is commonly used to derive three-dimensional structure elements.<sup>[21]</sup> Recently, renewed interest in  $^{13}\text{C}$  NMR spectroscopy has revealed structure–chemical shift relationships for the elucidation of the supramolecular structure of biomolecules.<sup>[22]</sup>

It is conceivable that when the indole moiety of a structurally defined Trp side chain is involved in  $\pi$  interactions, the noncovalent contact engaged by the indole ring could become constrained to an otherwise free rotamer interconversion of the natural Trp side chain.<sup>[16a]</sup>

Prior to this work,  $^{13}\text{C}$  NMR spectroscopic investigations demonstrated that  $\pi$  interactions involving indole side chains lead to a dynamic change in the Trp side-chain torsion angle.<sup>[16a]</sup>  $^{13}\text{C}$  NMR spectroscopy offers a window on dynamic changes in Trp side-chain torsion angle upon cation–indole bonding, and has the additional advantage of directly providing interaction information from different molecular scaffolds for comparison.<sup>[16a]</sup> In this work, structural change details associated with binding of diamagnetic metals were explored by  $^1\text{H}$  and  $^{13}\text{C}$  NMR spectroscopic studies, which permit the Trp side-chain dynamic interactions to be monitored in situ, including the His/Trp side-chain noncovalent contacts between the primary and secondary coordination spheres.

In the presence of one equivalent of metal ions at pH 7.1,  $^1\text{H}$  NMR spectra showed that metal binding caused a downfield shifting of H2 and H5 of the Im ring (Figure 1) as compared with the otherwise protonated form  $\text{ImH}^+$  in the apo form of the scaffolds. This downfield shift is accompanied by the upfield shifting of Im C(4) in the  $^{13}\text{C}$  NMR spectra (Figure 2). Because the positively charged metal centers are essentially coordinated by multivalent anionic carboxylate groups, the metal-bound imidazolium ring becomes less electron deficient than the  $\text{ImH}^+$  ring. The shifted resonance for both the protons (H2, H5) and carbon Im C(4) of the imidazole ring yields evidence that the metal is bound to the N3 imidazole nitrogen of the His residue,<sup>[4c,11d]</sup> which is indicated by the substantially smaller positive charge character on the N3 position of the  $\text{Im-M}^{\text{II}}$  ring in comparison to its protonated form  $\text{Im-H}^+$ .<sup>[23a]</sup>

Stable binding complexes of  $\text{Ca}^{2+}$  and  $\text{Mg}^{2+}$  ions coordinated with six and three imidazole rings, respectively, have been recently reported.<sup>[23b–d]</sup> The multivalency effect of the multiaminocarboxylate chelation framework within the peptidomimetic scaffolds might have further assisted the participation of an imidazole ring in the binding of  $\text{Ca}^{2+}$  and  $\text{Mg}^{2+}$  ions.

Concurrently, site-selective broadening of the Trp indolyl C3 resonance of both EWH and DWH in the presence of metal ions was apparent in the  $^{13}\text{C}$  NMR spectra (Figure 2), whereas the chemical shifts and signal pattern for the other indolyl carbon resonances remain nearly intact. This distinctively broad distribution of isotropic chemical shifts of equivalent carbon atoms (e.g., the Trp indolyl C3) is unambiguously diagnostic of drastically decreased mobility and restricted rotational motion of the indole side chain,<sup>[16a]</sup>

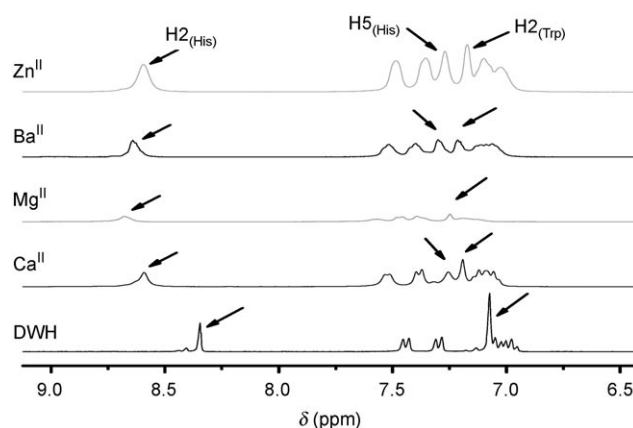
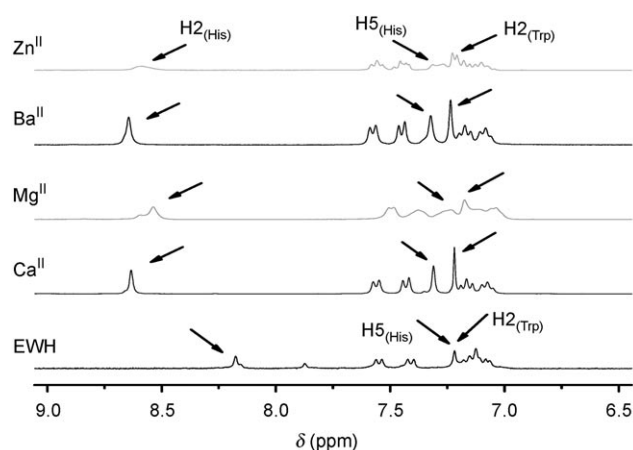


Figure 1. The H2 and H5 protons of the Im ring in metal-bound scaffolds  $M^{II}$ -EWH (top graph) and  $M^{II}$ -DWH (bottom graph) undergo downfield shifts as compared to the protonated Im ring of the apo-scaffolds in the absence of metal ions. See Scheme 2 for the atom numbering system.

which displays a slower rotamer interconversion rate (a frequency of  $\leq 10^8 \text{ s}^{-1}$ ) of Trp observed on the NMR spectroscopy timescale. The similar indole side-chain conformational fluctuation observed for both EWH and DWH suggests that cation- $\pi$  interactions predominantly arise from global interactions of the indole ring with the first coordination sphere (see below). In the absence of metals, a sharp singlet of indolyl C3 indicates fast averaging of the side-chain conformation on the NMR timescale when  $\pi$ -interaction is unavailable.

The signal broadening of the indole C3 together with small perturbations of the chemical shifts for the rest of aromatic carbon atoms of the indole moiety are indicative of the second-sphere indole ring being confined within a certain spatial orientation due to indole- $L^{\delta+}$ - $M^{II}$  electrostatic interactions,<sup>[5a-d,16a]</sup> rather than rapidly alternating rotamers between diverse orientations. Such cation-indole interactions resulted in energetically high Trp rotamers.<sup>[2]</sup>

$^{13}\text{C}$  NMR signals of aromatic carbons and carbonyl carbons and the  $^1\text{H}$  NMR spectrum allowed cross-validation of the participation of the imidazole, carboxylate, amide oxygen, and tertiary amino groups as primary metal ligands

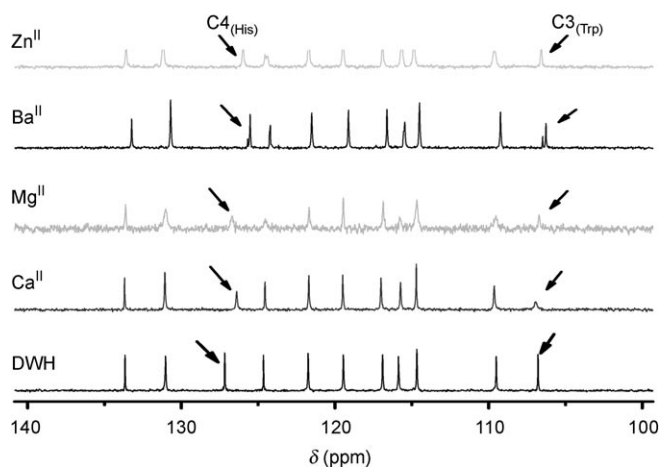
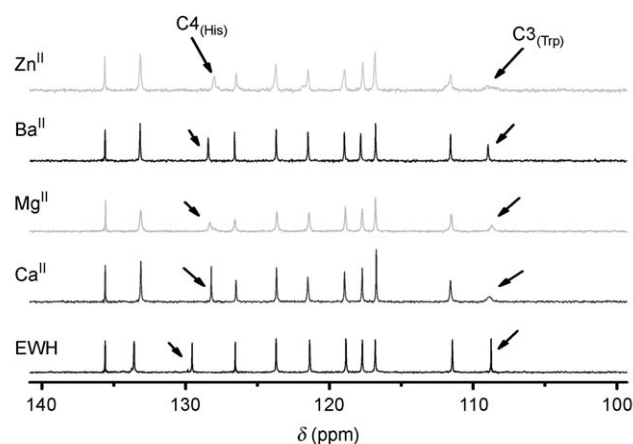


Figure 2. Site-selective broadening of the Trp indole C3 resonance in the  $^{13}\text{C}$  NMR spectra of  $M^{II}$ -EWH and  $M^{II}$ -DWH. The upfield shifting of Im C4 strongly indicated metal binding at the N3 of the Im ring, resulting in a transformation from  $\text{ImH}^+$  into  $\text{Im-M}^{II}$ . See Scheme 2 for the atom numbering system.

and indole as the secondary ligand in the binding of  $\text{Ca}^{2+}$ . The two ester carbonyl groups ( $\text{COOCH}_3$ ) were shown to be uninvolved in the metal-binding event (see the Supporting Information).

**Stereoisomerism and stereospecific orientation of aromatic rings:** Despite only one set of both  $^{13}\text{C}$  and  $^1\text{H}$  NMR spectroscopic signals clearly suggesting only one type of structure for an individual metal-bound scaffold and no linkage isomerism being observed, stereoisomerism of the metal-bound scaffolds can be exemplified by using the  $\text{Ca}^{2+}$ -EWH complex in solution.<sup>[24a]</sup>

In natural  $\text{Ca}^{2+}$ -binding sites of proteins, the  $\text{Ca}^{2+}$  ion is primarily coordinated by oxygen atoms;<sup>[24b,c]</sup> nevertheless, because the multivalency effect of the multiaminocarboxylate moiety substantially facilitates metal coordination by the imidazole ring N3 nitrogen, amide carbonyl oxygen, and backbone tertiary amino nitrogen groups, four diastereomeric pairs of conformers are possible for the octacoordinated  $\text{Ca}^{2+}$  complex.<sup>[21a,25,26]</sup>

Upon  $\text{Ca}^{2+}$  binding, two additional chiral centers are generated. Because the formation of a five-membered chelate ring is more favorable than a six-membered ring, which is in turn more favorable than a seven-membered ring, an octacoordinated structure in favor of the  $\text{N}_2\text{ImO}_4(\text{H}_2\text{O})$  coordination pattern can rationally be proposed for octacoordinated  $\text{Ca}^{2+}$  with EWH through two tertiary amino group nitrogen atoms, two monodentate carboxylate oxygen atoms, two monodentate amide carbonyl oxygen atoms, one imidazole ring nitrogen (N3), and one exchangeable (putative metal-bound) water molecule (Scheme 4).<sup>[24b,c]</sup>

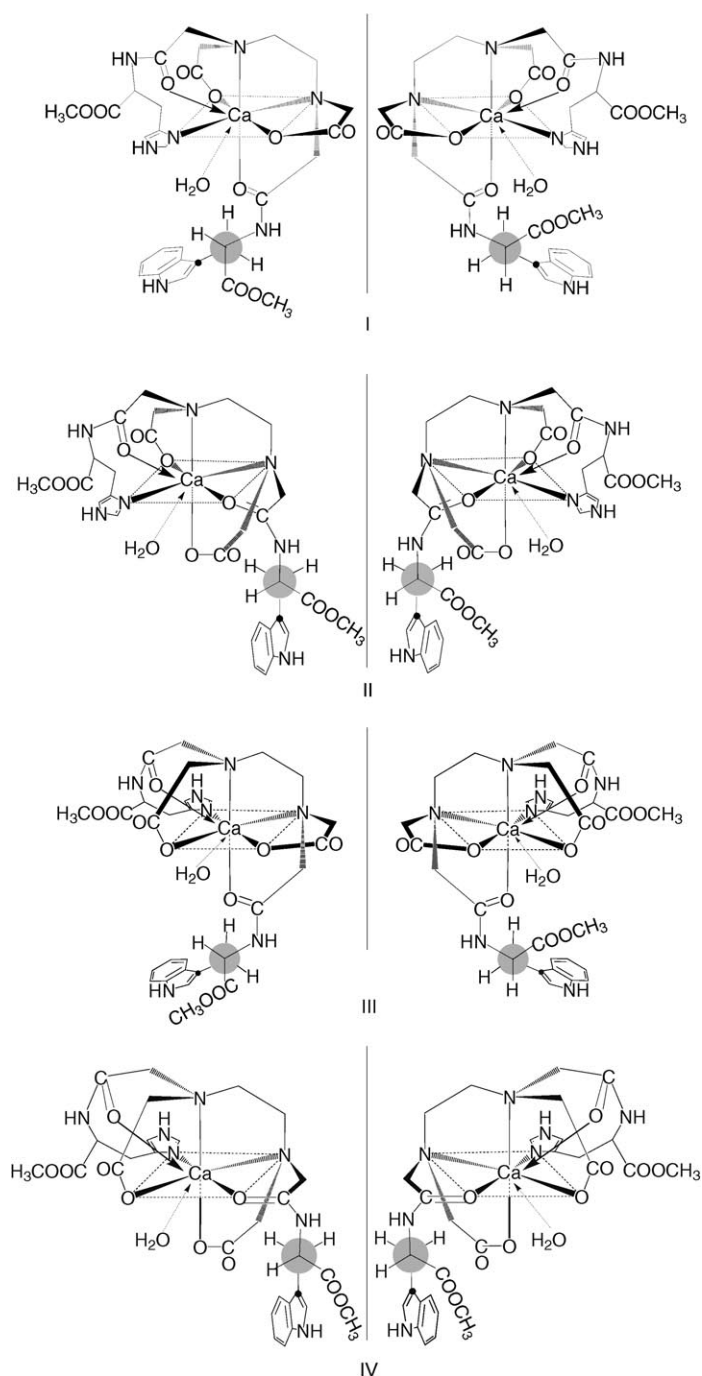
As indicated in Scheme 4, the two amino nitrogen atoms of the scaffold become chiral upon chelation, resulting in four diastereoisomers (*anti*-diamide/*syn*-diaromatic side chains; *anti*-diamide/*cis*-diaromatic side chains; *syn*-diamide/*syn*-di-side chains; *trans*-diamide/*anti*-di-side chains). Moreover, two enantiomers (wrapping isomers) exist for each diastereoisomer, resulting in eight stereoisomers for the  $\text{Ca}^{2+}$ –EWH complex. Within all the diastereoisomers, mutual orientations of the Im and indole side chains are stereospecifically confined through binding and noncovalent interactions.

Because the site-selective broadening of the Trp indolyl C3 resonance observed on the NMR timescale is accompanied by unchanged chemical shifts and signal pattern for the other indolyl carbons, the isotropic distribution of the otherwise equivalent Trp indolyl C3 resonance cannot be attributed to the above stereoisomerism, but to a restricted indole side-chain fluctuation (a frequency of  $\leq 10^8 \text{ s}^{-1}$ ) due to metal–indole attractions.

**Stereospecific  $\pi$  interactions and transient physicochemical properties:** Amino acid side-chain conformations can be described by their torsion angles. The preferred dihedral conformation for a residue type is termed a rotamer, which has been characterized as possessing configurations that represent a local minimum in potential energy and being associated with local, most favorable conformational entropy.<sup>[19,20,27a]</sup>

This study demonstrated the Trp side-chain conformational heterogeneity in metal-coordinating environment in aqueous solution.  $^{13}\text{C}$  NMR spectra offer a different method of illuminating the susceptibility of Trp side-chain rotamer interconversion to metal-coordination environment. Elucidating the role of dynamics and backbone and side-chain dependence of Trp rotamers may greatly benefit protein engineering experiments aimed at altering the metalloenzyme activity and function of metalloproteins.<sup>[28]</sup>

A Trp residue has six preferred rotamers: three  $\chi_1$  rotamers ( $\pm 60^\circ$  and  $180^\circ$ ) each with two  $\chi_2$  rotamers ( $\pm 90^\circ$ ).<sup>[20,27a]</sup> The conformational heterogeneity of Trp in native proteins due to Trp rotamers and the sensitivity to the secondary structure of the polypeptide main chain have been evidenced by X-ray crystallography, fluorescence lifetimes, NMR spectroscopy, and molecular dynamics modeling.<sup>[19a,29]</sup> Rotamer distributions are perturbed by the position of a Trp residue in a polypeptide.<sup>[29c]</sup> Marked deviations, which exist between NMR spectroscopic and X-ray datasets, are attributed to different rotameric states due to crystal-



Scheme 4. Four diastereoisomeric pairs of  $\text{Ca}^{2+}$ –EWH in idealized geometries (the  $\beta$ -carbon in Trp residue aligns toward the metal center): I) *anti*-diamide/*syn*-diaromatics, II) *anti*-diamide/*cis*-diaromatics, III) *syn*-diamide/*syn*-diaromatics, and IV) *trans*-diamide/*anti*-diaromatics.

packing effects and to conformational equilibria between multiple  $\chi_1$  rotamers.<sup>[29]</sup>

Because the fluorescence decay of Trp is a sensitive indicator of its local environment within a peptide or protein, the three  $\chi_1$  rotamers of the Trp side chain can be identified by their respective lifetime differences in the nanosecond range in fluorescence, with fluorescence lifetime heterogene-

ity being controlled by at least three ground-state rotamers with different lifetimes, with relative proportions of the lifetime components being related to the population and distribution of Trp  $\chi_1$  rotamers about the  $C_\alpha-C_\beta$  bond.<sup>[20c,27a-d]</sup>

To date, however, direct observation of Trp rotamer conversion has been impeded by a lack of spectroscopic measurements in which a visualization timescale is required to be comparable to rotamer interconversion rate. Herein  $^{13}\text{C}$  NMR spectra provided an unprecedented window for displaying Trp side-chain rotamer interconversion under cation- $\pi$  interactions in solution. The heterogeneous NMR Trp indole C3 signal revealed a frequency of  $\leq 10^8 \text{ s}^{-1}$  for the Trp side-chain fluctuations in the metal-bound state of the scaffolds, which is comparable with the rate constants for water exchange in metal-aqua ions, such as  $\text{Zn}^{2+}$ .<sup>[21a]</sup> In this respect interconversion between rotamers under cation- $\pi$  interactions are much slower than the nanosecond range of the fluorescence timescale, but comparable to the NMR spectroscopic timescale. Thus,  $^{13}\text{C}$  NMR provided a useful adjunct to other biophysical techniques for investigating Trp-containing biomolecules engaged in cation- $\pi$  noncovalent interactions.

The secondary structure and disposition of the Trp residue relative to the metal ions in the metallo complex can affect the local environment of Trp and influence the distribution of side-chain rotamers. The  $^{13}\text{C}$  NMR singlet of indolyl C3 for both EWH and DWH in the absence of metal ions displays the intrinsic rotamer distribution. In aqueous solution, the peptidomimetic scaffolds are unstructured, and EWH and DWH have flexible backbones, leaving natural side-chain rotamers as the only source of conformational heterogeneity. In this respect, the NMR spectra of either EWH or DWH in the absence of metal did not show signal broadening of the Trp indolyl C3, which is suggestive of signal broadening in the metal-bound state arising from a perturbed rotamer-conversion rate due to noncovalent interac-

tions (Figure 3). The reduced Trp rotamer flexibility is a parallel to the observed binding of the enzyme inhibitor acetylpepstatin to HIV-1 protease.<sup>[2a]</sup>

As shown by the  $^{13}\text{C}$  NMR spectroscopic study described above, natural Trp side-chain rotamers were perturbed by  $\pi$  interactions, providing definitive evidence for that backbone-dependent rotamers of Trp residues are sensitive to and strongly correlated to the electrostatic microenvironment. Because aromatic residue conformation and functionality are often intimately coupled to side-chain-specific interactions, certain higher-energy rotameric states due to local steric and pairwise electrostatic interactions have a potential in regulating protein functions.<sup>[2]</sup>

**NOE visualization of the Im-indole interplanar contact in  $\text{Ca}^{2+}$ -bound complexes:** Nuclear Overhauser enhancement (NOE) is useful to determine the electronic effect on intramolecular  $\pi$  interactions.<sup>[30]</sup> Because  $\text{Ca}^{2+}$  ions possess a high coordination number with a flexible coordination sphere geometry, combined with simple electronic properties with respect to routine NMR spectroscopy in a structural measurement,  $\text{Ca}^{2+}$ -bound states in solution were subjected to 2D NMR spectroscopic investigation for an in-depth inspection of the Im/indole ring interplanar orientation and contact. The observed NOE between the Im<sup>+</sup> and indole units requires a particular orientation of the indole ring nitrogen relative to the Im ring.

In this regard, prior to carrying out an NOE study the protonation-deprotonation property of histidine Im ring in the scaffolds was investigated by using a deuterium isotope-exchange experiment. The APT  $^{13}\text{C}$  NMR spectrum helped to demonstrate that the H5 of Im ring is available for NOE examination of binding in  $\text{D}_2\text{O}$ -containing solvent (see the Supporting Information). The H2 and H5 protons of Im ring were found to be partially deuterated, illustrating that H2 is more susceptible to isotope exchange than H5. Both  $^1\text{H}$  NMR and APT  $^{13}\text{C}$  NMR spectroscopy revealed that the relative strength of proton acidity is  $\text{N-H1} > \text{C-H2} > \text{C-H5}$  in the Im ring.

The NOESY spectrum of  $\text{Ca}^{2+}$ -EWH exhibited connectivity between the aromatic proton resonances of indolyl C-H2 (Trp) and Im<sup>+</sup> C-H5 (Im- $\text{Ca}^{2+}$ ;  $\delta = 7.25 \text{ ppm}$ ; see Figure 4), which is consistent with the indole unit being oriented toward the Im ring through a severely distorted stacking (see MMFF structure below), with a distance between the C-H2(indolyl) and C-H5(Im<sup>+</sup>) being estimated to be about 4.8–5.0 Å by NMR spectroscopy. The evident NOE cross-peak between the side-chain rings of His and Trp corroborate an alignment in which the Im<sup>+</sup> moiety is perpendicular (orthogonal) to the pyrrole ring of the indole moiety, namely, a T-shaped (edge-to-face) alignment (Scheme 5), irrespective of the presence of polar solvent (e.g., water).<sup>[8a,b,h]</sup> This  $\pi^+-\pi$  contact is feasible because the Im<sup>+</sup> ring is equivalent to a substituted aromatic ring;<sup>[8]</sup> moreover, this interactive mode is generally consistent with a previous finding that a metal-bound Im<sup>+</sup> ring cation preferably contacts with the pyrrolo subunit rather than the indole benzene ring.<sup>[31]</sup>

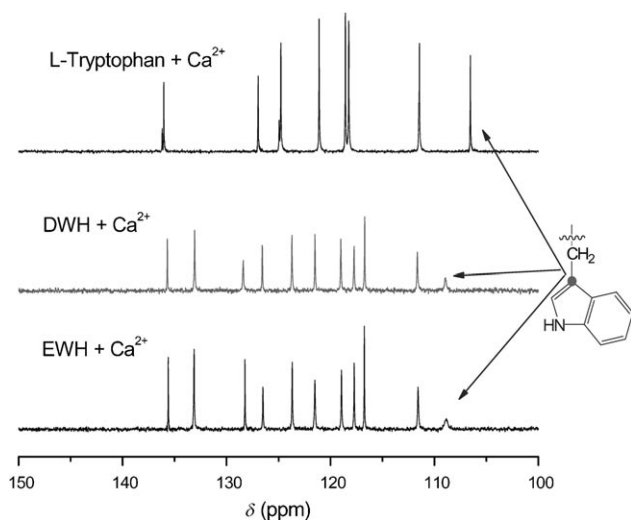


Figure 3. A comparison of the aromatic regions of the  $^{13}\text{C}$  NMR spectra of the  $\text{Ca}^{2+}$ -bound states of EWH, DWH, and L-tryptophan in  $\text{D}_2\text{O}/[\text{D}_6]\text{DMSO}$  1:1 (v/v), 25.0°C.  $\text{Ca}^{2+}$  binding resulted in site-selective signal broadening of the Trp indolyl C3.



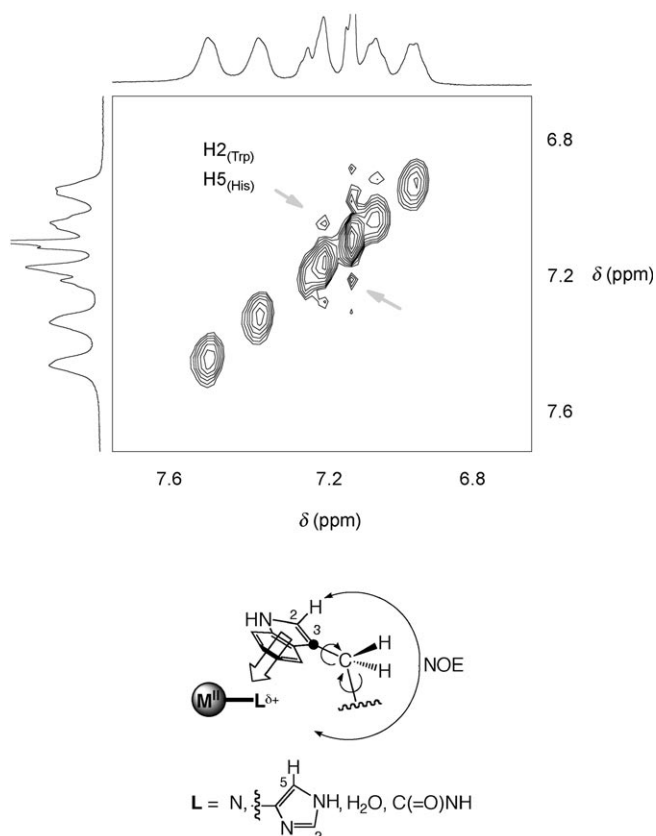
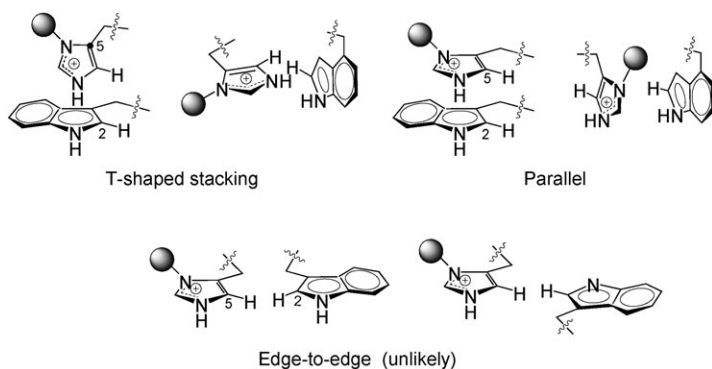


Figure 4. NOEs between the indole and imidazolium rings in the NOESY spectrum of  $Ca^{2+}$ –EWH.



Scheme 5. Orientation-dependent  $\pi$ – $\pi$  interaction modes in the idealized geometries of the T-shaped, parallel, and edge-to-edge alignments, derived on the basis of NOEs between C–H2(Indole) and C–H5(Im).

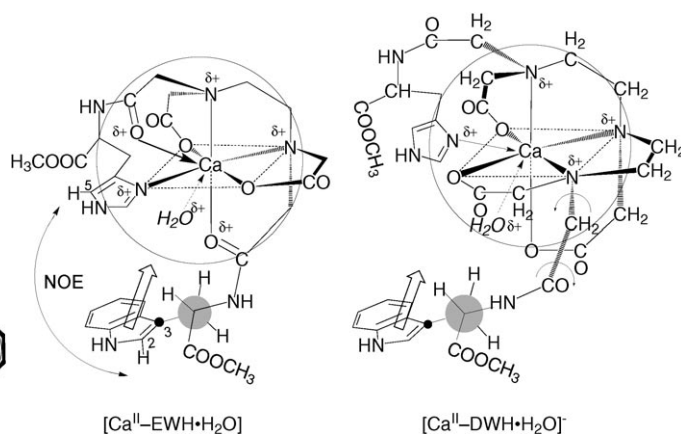
Considered together with all the energetically favorable T-shaped and parallel stacking arrangements between the Im and indole rings (see below), the NOE essentially suggests that the N–H1 of the  $Im^+-M^{II}$  ring points towards the pyrrole ring of the indole unit in the most likely edge-to-face  $\pi^+-\pi$  alignment (Scheme 5).<sup>[8]</sup> Although the  $\pi^+-\pi$  alignment could distort from its idealized geometries, this previously unprecedented interaction mode can be rationalized by the notion that the N1,3 and C2 atoms of the metal-

bound Im ring carry partial positive charges due to resonance that occurs when N3 is bound to a metal cation. This unique T-shaped  $\pi^+-\pi$  alignment can mechanistically explain an earlier finding that a Trp/His-containing metal site can facilitate hydrogen-atom tunneling in metalloproteins.<sup>[6f]</sup>

Thus, after the binding of  $Ca^{2+}$  to the Im N3 in the  $Ca^{2+}$ –EWH complex, the electron-rich indole ring comes into contact with the metal-bound, positively charged  $Im^+$  ring, with the distance between C–H2(indole) and C–H5(Im) being within the range of noncovalent interactions.

Because the analysis of chemical shifts, especially NOEs, is a reliable method for identifying cation– $\pi$  interactions in dynamic systems,<sup>[30]</sup> the NOE and the concomitant perturbations of chemical shifts and site-selective  $^{13}C$  NMR indolyl C3 spectroscopic signal broadening are clearly manifesting the dynamic  $Im^+-\pi$  electrostatic interaction across the secondary coordination sphere in the  $Ca^{2+}$ –EWH complex.

In contrast, no discernible NOE was observed in the corresponding  $Ca^{2+}$ –DWH complex, which is however in conformity with the energy-minimized structure (MMFF, see below), displaying a long-range spatial arrangement between the two aromatic rings (Scheme 6).<sup>[32]</sup> The lack of NOE in



Scheme 6. Coordinating modes for  $Ca^{2+}$  binding to EWH (left) and DWH (right). In the  $Ca^{2+}$ –EWH complex, binding of the Trp peptidyl amide oxygen to the metal enabled the Trp side-chain indole to be locked in a particular orientation relative to the  $Im^+$  ring. NOEs were observed in  $Ca^{2+}$ –EWH, but not in  $Ca^{2+}$ –DWH. The structures are derived from  $^1H$  and  $^{13}C$  NMR, and NOE spectra.  $^{13}C$  NMR spectroscopy showed that two methoxycarbonyl groups  $COOCH_3$  do not participate in the coordination, see the Supporting Information.

the  $Ca^{2+}$ –DWH complex is not unexpected. This observation is due in part to the extra aminocarboxylate group in the DWH scaffold, which ensures that not all the amide groups of the DWH are required for binding to the metal ions and thereby leaves the flexible Trp side chain unable to be confined in a restricted position towards the  $Ca^{2+}$ -bound  $Im^+$  ring. Putative coordinating modes are described in Scheme 6.

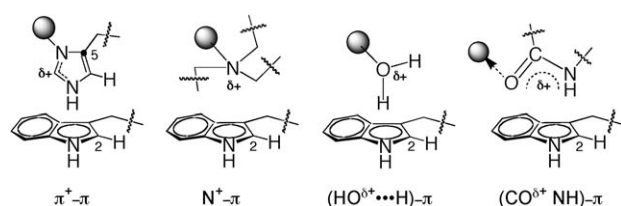
Furthermore, because there were no other NOEs arising from either the indole protons of Trp or Im of His, it is clear that the Trp side chain in both  $Ca^{2+}$ –EWH and  $Ca^{2+}$ –DWH



still attain multiple, albeit sterically constrained, rotamer conformations in its respective sites.

In parallel to this study, we have established that, depending on the type of bound metal, the local electronic and steric nature of neighboring aromatic residues in the second coordination sphere not only modulate the conformational structure of metal sites for stereospecific microenvironmental adaptation, but also transiently regulate electron-cloud distribution in a dynamic network surrounding the first coordination sphere.<sup>[33]</sup>

In light of the above findings obtained from the combined fluorescence, <sup>13</sup>C and <sup>1</sup>H NMR spectroscopic characterization, individual cation- $\pi$  interaction components involving a Trp side-chain indole  $\pi^+-\pi$ ,  $N^+-\pi$ ,  $(HO^{\delta+}\cdots H)-\pi$ , and  $(CO^{\delta+}NH)-\pi$  were accordingly suggested (Scheme 7). In ad-



Scheme 7. Individual cation- $\pi$  interaction components involving a Trp indole.

dition to the  $\pi^+-\pi$  interactions identified in  $Ca^{2+}$ -EWH, competitive noncovalent bonding modes include  $M^{II}\cdots N^+-\pi$  interactions.<sup>[1e,5,16a,b,34]</sup> As depicted in Schemes 6 and 7, the metal-bound tertiary ammonium entity, which acquired partial positive charge as a result of  $M^{II}$ -aminocarboxylate chelation, interacts with the  $\pi$  surface of a second-shell Trp aromatic side chain. In addition, charge-assisted  $(HO\cdots H)^{\delta+}-\pi$ <sup>[5a-d]</sup> and  $(CO\cdots NH)^{\delta+}-\pi$ <sup>[16a,b,35]</sup> interactions may compete with the  $M^{II}\cdots N^+-\pi$  and  $\pi^+-\pi$  interactions as the positive charge on divalent  $M^{II}$  became distributed among the metal-bound tertiary nitrogen atoms, amide moiety (CONH), and a putative, metal-bound water molecule depending on the buffer and/or pH upon metalloscaffold formation.

#### MMFF calculations of an imidazole/indole orientation

**An intramolecular imidazolium ( $\pi^+$ )-indole ( $\pi$ ) orientation in the metalloscaffolds:** Empirical potential energy calculations by using the energy minimization technique through molecular mechanics force field calculations (Spartan'08)<sup>[32]</sup> predicted that the frameworks positioned a distal Trp indole moiety proximal to a metal-bound Im cationic entity in the energetically most stable conformations of the metal-bound scaffolds (Figure 5). Variation can also be observed in the orientation of the Trp side chain with respect to the Im ring. Moreover, MMFF calculations demonstrate that the relative orientation and interactions between the side-chain Im and indole rings in the intramolecularly stacked conformers are highly dependent on metal-ion coordination number and ge-

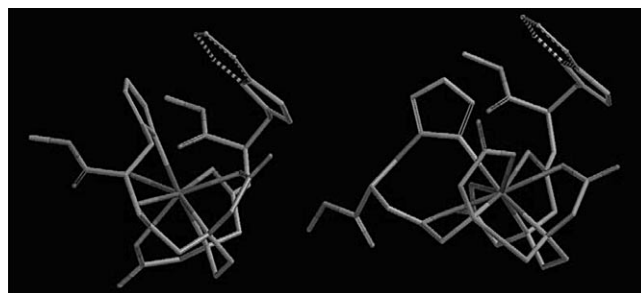


Figure 5. Energy-minimized structures of  $[Ca^{2+}-EWH\cdot H_2O]$  (left) and  $[Ca^{2+}-DWH\cdot H_2O]$  (right), calculated by using MMFF (Spartan'08).<sup>[32]</sup> Hydrogen atoms are omitted for clarity. The coordination numbers of  $Ca^{2+}$  in the two metallo-complexes are eight and nine, respectively.<sup>[21a,24b,c]</sup>

ometry, and constrained by the cooperative interactions surrounding the metal centers.

**A comparative study using intermolecular, parallel versus T-shaped, stacking between the free Trp/His residues:** To rationalize how His and Trp side-chain aromatic rings interact in the most favorable way from both thermodynamic and entropic points of view, a structure-based computational search was carried out from all types of possible intermolecular alignments between the two free amino acid residues, *N*-acetyl-L-tryptophan amide and the Im-protonated form of *N*-acetyl-L-histidine amide. During the search, it was assumed that the free energy surface of the hypothetical Trp/His side-chain complex is defined by the angle between the aromatic rings and by the distance between the centroids of the aromatic rings.<sup>[36]</sup>

Eight types of canonical, idealized parallel stacking between Im and indole ring side chains existed that fulfilled the NOE requirement between C-H2(indole) and C-H5(Im). Although it was found that the most-favorable alignment (in column 2, Figure 6) for aromatic rings is the one in which NH of the ImH<sup>+</sup> unit points to pyrrolo N1-H, which is in accord with the parallel stacking interactions depicted in Scheme 5, nevertheless, the amino acid backbones are highly sterically hindered.

Meanwhile, six types of canonical, idealized T-shaped (orthogonal) spatial arrangements were obtained that fulfilled the observed NOE requirement. All these arrangements can

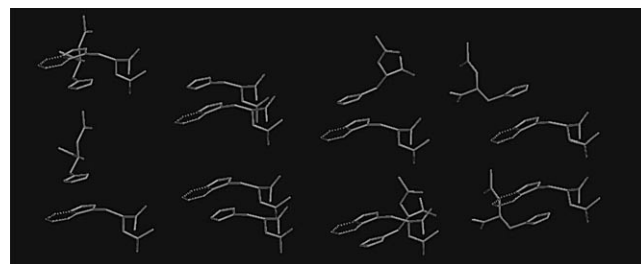


Figure 6. Parallel stacking between the Im and Indole side chains in idealized geometries.<sup>[32]</sup>

be merged to an alignment in which NH of the ImH<sup>+</sup> unit points to pyrrolo unit. The most energetically favorable alignment (shown in Figure 7, column 3) is actually in accord with the suggested T-shaped arrangement as depicted in Scheme 5.

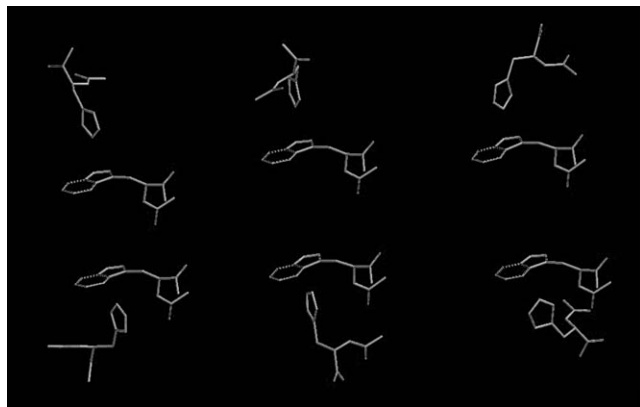


Figure 7. T-shaped stacking between the Im and Indole side chains in idealized geometries.

## Conclusion

Though Trp/His side-chain interactions have held the interest of chemists for years and a number of theoretical studies have been reported on indole/imidazole orientation in proteins, much is still to be learned about the physicochemical basis of functional and mechanistic versatility conferred by a metal-site Trp/His pair. Our work herein on Trp/His-containing biomimetic constructs, which mimic mononuclear metal-binding sites, permitted an exploration of indole–imidazole side-chain orientation and stereospecific  $\pi$  interactions across the first and second coordination spheres of bio-metal ions by <sup>1</sup>H and <sup>13</sup>C NMR spectroscopy. The binding feature and identities of the metal-bound complexes with a stoichiometry of 1:1 were investigated by using <sup>1</sup>H and <sup>13</sup>C NMR spectroscopy, which facilitated a cross-validation of the carboxylate, amide oxygen, and tertiary amino groups as the primary ligands and indole as the secondary ligand, with the Im N3 nitrogen also being weakly bound to metals such as Ca<sup>2+</sup> owing to a multivalency effect. Surrounding the metal centers, the stereospecific orientation of the hydrophobic and hydrophilic bioaromatic rings is interpreted in the diastereoisomerism, as exemplified by using the Ca<sup>2+</sup>–EWH complex. With respect to the perturbed Trp side-chain rotamer heterogeneity, unambiguous evidence for a drastically restricted Trp side-chain flexibility and thus a dynamically constrained rotamer interconversion due to a  $\pi$  interaction is provided by the site-selective <sup>13</sup>C NMR signal broadening of Trp indolyl C3. Furthermore, effects of Trp side-chain fluctuation on indole–Im interactions were the subject of a 2D NMR spectroscopy study of the Ca<sup>2+</sup>-bound state in solution, coupled with deuterium isotope-exchange experiments; a C–H2(indolyl)/C–H5(Im<sup>+</sup>) connectivity ob-

served in the NOESY spectra captured direct evidence that the N–H1 of the Ca<sup>2+</sup>–Im<sup>+</sup> unit interacts with the pyrrole ring of the indole unit in the Ca<sup>2+</sup>-bound state of EWH, which is assignable to a moderately static, anomalous T-shaped interplanar  $\pi^+ - \pi$  stacking alignment. This unique  $\pi^+ - \pi$  alignment might form an aromatic-recognition interface and mechanistically facilitates hydrogen-atom tunneling in metalloproteins. Nevertheless, a comparative <sup>13</sup>C NMR spectroscopic study of the two homologous scaffolds revealed that the overall response of the indole unit arises predominantly from global attractions between the indole aromatic ring and the entire positively charged first coordination sphere. Through MMFF calculations, the conformational variations and dynamic physicochemical structure involving Trp and His side-chain interactions, which integrate the primary and secondary coordination spheres, can be shown to be specific to the type of bound metal. The study thus established a coordination-sphere/geometry dependence of Trp–His side-chain interactions in forming an aromatic recognition interface surrounding metal centers. Because cation– $\pi$  interactions drastically restrict rotational motion of the indole side chain, thereby slowing down the Trp rotamer-interconversion rate, the study demonstrated that  $\pi$  interactions surrounding metal-binding centers enabled <sup>13</sup>C NMR spectroscopy to offer a new, alternative method for visualizing Trp side-chain conformation heterogeneity due to restricted rotamer interconversion, and illuminated that such restricted rotamer-interconversion rates ( $\leq 10^8$  s<sup>-1</sup>) are on the NMR spectroscopic timescale (that is, approaching microsecond-timescale motions). As a result, the biomimetic metal–motif mimicry offered a novel vehicle for spectroscopic observation of perturbed rotamer interconversion as restricted by metal-induced electrostatic interactions, and provided a previously intractable design for high-energy Trp rotamers.

## Experimental Section

**Materials:** D<sub>2</sub>O (99.95%) was obtained from Acros and [D<sub>6</sub>]DMSO was purchased from Aldrich and both were used as received. All other solvents and reagents, including CH<sub>2</sub>Cl<sub>2</sub> and Et<sub>3</sub>N, were of analytical grade and were dried and purified before use. EWH and DWH were synthesized by following our recently described procedure.<sup>[16]</sup> The analytical purity of EWH and DWH was further ascertained by HPLC and <sup>13</sup>C NMR identification of the six types of C=O groups in EWH and seven types of C=O groups in DWH. For NMR spectra and MMFF calculation structures, see the Supporting Information.

**Spectroscopic methods:** <sup>1</sup>H and <sup>13</sup>C NMR spectra and NOE were recorded by using a VARIAN UNITY-plus 400 spectrometer. Electrospray ionization mass spectrometry data (ESI-MS) were collected by using a Finnigan LCQ-Advantage 10 grade ion-trap LC-MS, and the flow rate of the LC pump was 4 mL min<sup>-1</sup>. Divalent ions were screened for binding under similar conditions. Molecular mechanics force field calculations were carried out by using the PC software Spartan'08.<sup>[32]</sup>

**2D NMR (NOESY) spectra of the Ca<sup>2+</sup> complex:** NOESY spectra of the aromatic regions of Ca<sup>2+</sup>–EWH (Figure 8) and Ca<sup>2+</sup>–DWH (Figure 9) in D<sub>2</sub>O/[D<sub>6</sub>]DMSO 1:1 (v/v), 25.0°C, were obtained and compared.

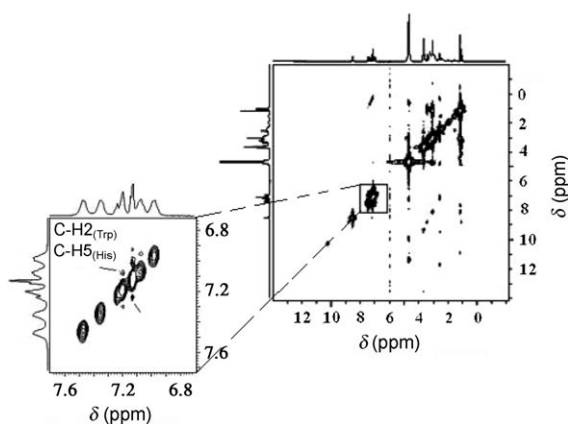


Figure 8. NOESY spectrum of Ca<sup>2+</sup>-EWH.

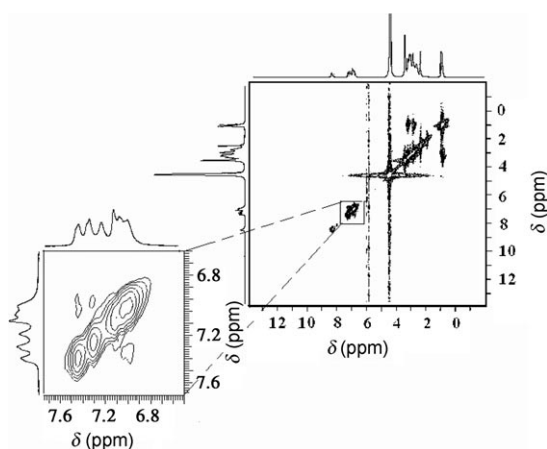


Figure 9. NOESY spectrum of Ca<sup>2+</sup>-DWH.

## Acknowledgements

We acknowledge funding of this work by the NSF China (nos. 20042002, 20472029, 20421202) and also the generous support from Tongji University. Laboratory and experimental assistance from students Meng Zhang, Manman Lu, Xiaoqing Shi, and Zhipeng Sun are appreciated. The authors also express appreciation for several *Chimia* journal issues received from Professor Jay S. Siegel (University of Zurich), which were helpful to the study, and thank an anonymous referee for insightful suggestions.

- [1] a) M. Karplus, J. Kuriyan, *Proc. Natl. Acad. Sci. USA* **2005**, *102*, 6679; b) B. A. Shoemaker, A. R. Panchenko, *PLoS Comput. Biol.* **2007**, *3*, 595; c) C. L. Vizcarra, S. L. Mayo, *Curr. Opin. Chem. Biol.* **2005**, *9*, 622; d) W. L. Delano, *Curr. Biol.* **2002**, *12*, 14; e) E. A. Meyer, R. K. Castellano, F. Diederich, *Angew. Chem.* **2003**, *115*, 1244; *Angew. Chem. Int. Ed.* **2003**, *42*, 1210; f) Y. Xue, A. V. Davis, G. Balakrishnan, J. P. Stasser, B. M. Staehlin, P. Focia, T. G. Spiro, J. E. Penner-Hahn, T. V. O'Halloran, *Nat. Chem. Biol.* **2008**, *4*, 107.
- [2] a) B. Ullrich, M. Laberge, F. Tölgyesi, J. Fidy, Z. Szeltner, L. Polgár, *Protein Sci.* **2000**, *9*, 2232; b) E. Alexov, *Proteins Struct. Funct. Bioinf.* **2003**, *50*, 94; c) S. D. McAllister, D. P. Hurst, J. Barnett-Norris, D. Lynch, P. H. Reggio, M. E. Abood, *J. Biol. Chem.* **2004**, *279*, 48024; d) R. L. Dunbrack, Jr., *Curr. Opin. Struct. Biol.* **2002**, *12*, 431; e) G. L. Butterfoss, J. Hermans, *Protein Sci.* **2003**, *12*, 2719.
- [3] a) M. S. Rogers, E. M. Tyler, N. Akyumani, C. R. Kurtis, R. K. Spooner, S. E. Deacon, S. Tamber, S. J. Firbank, K. Mahmoud, P. F. Knowles, S. E. V. Phillips, M. J. McPherson, D. M. Dooley, *Biochemistry* **2007**, *46*, 4606; b) D. Rokhsana, D. M. Dooley, R. K. Szilagyi, *J. Biol. Inorg. Chem.* **2008**, *13*, 371.
- [4] S. Yanagisawa, P. B. Crowley, S. J. Firbank, A. T. Lawler, D. M. Hunter, W. McFarlane, C. Li, T. Kohzuma, M. J. Banfield, C. Dennison, *J. Am. Chem. Soc.* **2008**, *130*, 15420.
- [5] a) S. D. Zarić, D. M. Popović, E.-W. Knapp, *Chem. Eur. J.* **2000**, *6*, 3935; b) O. Yamauchi, A. Odani, M. Takani, *J. Chem. Soc. Dalton Trans.* **2002**, *18*, 3411; c) S. D. Zarić, *Eur. J. Inorg. Chem.* **2003**, 2197; d) H. Kumita, T. Kato, K. Jitsukawa, H. Einaga, H. Masuda, *Inorg. Chem.* **2001**, *40*, 3936; e) S. Novokmet, F. W. Heinemann, A. Zahl, R. Alsasser, *Inorg. Chem.* **2005**, *44*, 4796; f) D. Liu, D. A. Williamson, M. L. Kennedy, T. D. Williams, M. M. Morton, D. R. Benson, *J. Am. Chem. Soc.* **1999**, *121*, 11798; g) N. J. van der Veen, R. J. M. Egberink, J. F. J. Engbersen, F. J. C. M. van Veggel, D. N. Reinhoudt, *Chem. Commun.* **1999**, 681; h) D. W. Christianson, *Prog. Biophys. Mol. Biol.* **1997**, *67*, 217; i) J.-H. Lim, Y. G. Yu, Y. S. Han, S.-J. Cho, B.-Y. Ahn, S.-H. Kim, Y. Cho, *J. Mol. Biol.* **1997**, *270*, 259; j) T. Ursby, B. S. Adinolfi, S. Al-Karadaghi, E. De Vendittis, V. Bocchini, *J. Mol. Biol.* **1999**, 286, 189.
- [6] a) H. X. Deng, A. Hentati, J. A. Tainer, Z. Iqbal, A. Cayabyab, W. Y. Hung, E. D. Getzoff, P. Hu, B. Herzfeldt, R. P. Roos, *Science* **1993**, *261*, 1047; b) M. E. Winkler, R. D. Sereman, *J. Am. Chem. Soc.* **1980**, *102*, 6244; c) A. Okada, T. Miura, H. Takeuchi, *Biochemistry* **2001**, *40*, 6053; d) J. M. Matthews, L. D. Ward, A. Hammacher, R. S. Norton, R. J. Simpson, *Biochemistry* **1997**, *36*, 6187; e) D. Batabyal, S.-R. Yeh, *J. Am. Chem. Soc.* **2009**, *131*, 3260; f) B. J. Bahnson, T. D. Colby, J. K. Chin, B. M. Goldstein, J. P. Klinman, *Proc. Natl. Acad. Sci. USA* **1997**, *94*, 12797.
- [7] a) G. L. Millhauser, *Acc. Chem. Res.* **2004**, *37*, 79; b) G. L. Millhauser, *Annu. Rev. Phys. Chem.* **2007**, *58*, 299; c) M. Gustiananda, J. R. Liggins, P. L. Cummins, J. E. Gready, *Biophys. J.* **2004**, *86*, 2467; d) E. S. Riihimäki, J. M. Martínez, L. Kloo, *Phys. Chem. Chem. Phys.* **2008**, *10*, 2488; e) E. D. Walter, D. J. Stevens, M. P. Visconte, G. L. Millhauser, *J. Am. Chem. Soc.* **2007**, *129*, 15440; f) H. Yoshida, N. Matsushima, Y. Kumaki, M. Nakata, K. Hikichi, *J. Biochem.* **2000**, *128*, 271; g) F. H. Ruiz, E. Silva, N. C. Inestrosa, *Biochem. Biophys. Res. Commun.* **2000**, *269*, 491; h) S. R. Leliveld, L. Stitz, C. Korth, *Biochemistry* **2008**, *47*, 6267; i) C. M. Yang, *Abstr. Pap. Am. Chem. Soc.* **2000**, 220, U224; j) C. M. Yang, *Biochemistry* **2003**, *42*, 8633.
- [8] a) A. Mukherjee, B. Bagchi, *Biochemistry* **2006**, *45*, 5129; b) L. Brocchieri, S. Karlin, *Proc. Natl. Acad. Sci. USA* **1994**, *91*, 9297; c) R. Chelli, F. L. Gervasio, P. Procacci, V. Schettino, *J. Am. Chem. Soc.* **2002**, *124*, 6133; d) J. Fernández-Recio, A. Vázquez, C. Civera, P. Sevilla, J. Sancho, *J. Mol. Biol.* **1997**, *270*, 535; e) G. Alagona, C. Ghio, S. Monti, *J. Phys. Chem. A* **1998**, *102*, 6152; f) J. Fernández-Recio, A. Vázquez, C. Civera, P. Sevilla, J. Sancho, *J. Mol. Biol.* **1997**, *267*, 184; g) F. L. Gervasio, V. Schettino, S. Mangani, M. Krack, P. Carloni, M. Parrinello, *J. Phys. Chem. B* **2003**, *107*, 6886; h) F. R. Fisher, W. B. Schweizer, F. Diederich, *Chem. Commun.* **2008**, 4031; i) F. J. Carver, C. A. Hunter, D. J. Livingstone, J. F. McCabe, E. M. Seward, *Chem. Eur. J.* **2002**, *8*, 2848; j) L. Wang, N. Sun, S. Terzyan, X. Zhang, D. R. Benson, *Biochemistry* **2006**, *45*, 13750.
- [9] a) *Handbook on Metalloproteins* (Eds.: I. Bertini, A. Sigel, H. Sigel), Marcel Dekker, New York, **2001**; b) A. Messerschmidt, R. Huber, T. Poulos, K. Wieghardt, *Handbook of Metalloproteins*, Wiley, New York, **2001**; c) M. M. Yamashita, L. Wesson, G. Eisenman, D. Eisenberg, *Proc. Natl. Acad. Sci. USA* **1990**, *87*, 5648; d) D. E. Benson, M. S. Wisz, H. W. Hellinga, *Curr. Opin. Chem. Biol.* **1998**, *2*, 370; e) R. J. P. Williams, *Chem. Commun.* **2003**, 1109.
- [10] a) E. N. Salgado, J. Faraone-Mennella, F. A. Tezcan, *J. Am. Chem. Soc.* **2007**, *129*, 13374; b) M. Gochin, R. K. Guy, M. A. Case, *Angew. Chem.* **2003**, *115*, 5483; *Angew. Chem. Int. Ed.* **2003**, *42*, 5325; c) B. T. Farrer, V. L. Pecoraro, *Proc. Natl. Acad. Sci. USA* **2003**, *100*, 3760; d) L. Zhang, Y. Wu, L. Brunsfeld, *Angew. Chem.* **2007**, *119*,

- 1830; *Angew. Chem. Int. Ed.* **2007**, *46*, 1798; e) E. N. Salgado, R. A. Lewis, J. Faraone-Mennella, F. A. Tezcan, *J. Am. Chem. Soc.* **2008**, *130*, 6082; f) R. J. Radford, F. A. Tezcan, *J. Am. Chem. Soc.* **2009**, *131*, 9136.
- [11] a) A. F. A. Peacock, L. Hemmingsen, V. L. Pecoraro, *Proc. Natl. Acad. Sci. USA* **2008**, *105*, 16566; b) S. B. Shields, S. J. Franklin, *Biochemistry* **2004**, *43*, 16086; c) M. Albrecht, P. Stortz, *Chem. Soc. Rev.* **2005**, *34*, 496; d) E. Gaggelli, N. D'Amelio, D. Valensin, G. Valensin, *Magn. Reson. Chem.* **2003**, *41*, 877; e) Y. Lu, S. M. Berry, T. D. Pfister, *Chem. Rev.* **2001**, *101*, 3047; f) C. M. Thomas, T. R. Ward, *Chem. Soc. Rev.* **2005**, *34*, 337; g) S. C. Burdette, S. J. Lippard, *Coord. Chem. Rev.* **2001**, *216*, 333; h) B. R. Sculimbrene, B. Imperiali, *J. Am. Chem. Soc.* **2006**, *128*, 7346; i) C. W. V. Hogue, J. P. MacManus, D. Banville, A. G. Szabo, *J. Biol. Chem.* **1992**, *267*, 13340; j) W. S. Wade, J. S. Koh, N. Han, D. M. Hoekstra, R. A. Lerner, *J. Am. Chem. Soc.* **1993**, *115*, 4449.
- [12] a) C. Shih, A. K. Museth, M. Abrahamsson, A. M. Blanco-Rodriguez, A. J. Di Bilio, J. Sudhamsu, B. R. Crane, K. L. Ronayne, M. Towrie, A. Vlcek, Jr., J. H. Richards, J. R. Winkler, H. B. Gray, *Science* **2008**, *320*, 1760; b) J. M. Bollinger, Jr., *Science* **2008**, *320*, 1730; c) J. E. Miller, C. Grodinaru, B. R. Crane, A. J. Di Bilio, W. Wehbi, S. Un, J. R. Winkler, H. B. Gray, *J. Am. Chem. Soc.* **2003**, *125*, 14220; d) M. Cordes, B. Giese, *Chem. Soc. Rev.* **2009**, *38*, 892.
- [13] a) B. W. Berry, M. M. Elvekrog, C. Tommos, *J. Am. Chem. Soc.* **2007**, *129*, 5308; b) J. Ramos, T. Lazaridis, *J. Am. Chem. Soc.* **2007**, *129*, 15499; c) J. Liu, W. Yong, Y. Deng, N. R. Kallenbach, M. Lu, *Proc. Natl. Acad. Sci. USA* **2004**, *101*, 16156.
- [14] a) J. P. Gallivan, D. A. Dougherty, *Proc. Natl. Acad. Sci. USA* **1999**, *96*, 9459; b) S. Mecozzi, A. P. West, Jr., D. A. Dougherty, *Proc. Natl. Acad. Sci. USA* **1996**, *93*, 10566.
- [15] a) J. A. Robinson, *ChemBioChem* **2009**, *10*, 971; b) P. H. Kussie, S. Gorina, V. Marechal, B. Elenbaas, J. Moreau, A. J. Levine, N. P. Pavletich, *Science* **1996**, *274*, 948; c) O. Rosen, M. Sharon, S. R. Quadt-Akabayov, J. Anglister, *Proc. Natl. Acad. Sci. USA* **2006**, *103*, 13950; d) S. Ricagno, M.-P. Egloff, R. Ulferts, B. Coutard, D. Nurizzo, V. Campanacci, C. Cambillau, J. Ziebuhr, B. Canard, *Proc. Natl. Acad. Sci. USA* **2006**, *103*, 11892; e) R. J. Abergel, M. K. Wilson, J. E. L. Arceneaux, T. M. Hoette, R. K. Strong, B. R. Byers, K. N. Raymond, *Proc. Natl. Acad. Sci. USA* **2006**, *103*, 18499; f) M. Tantama, S. Licht, *ACS Chem. Biol.* **2008**, *3*, 693.
- [16] a) Y. Li, C. M. Yang, *J. Am. Chem. Soc.* **2005**, *127*, 3527; b) C. M. Yang, X. Li, W. Wei, Y. Li, Z. Duan, J. Zheng, T. Huang, *Chem. Eur. J.* **2007**, *13*, 3120; c) Y. Li, C. M. Yang, *Chem. Commun.* **2003**, 2884.
- [17] a) A. Mulder, T. Auletta, A. Sartori, S. Del Ciotto, A. Casnati, R. Ungaro, J. Huskens, D. N. Reinhoudt, *J. Am. Chem. Soc.* **2004**, *126*, 6627; b) J. J. Michels, J. Huskens, D. N. Reinhoudt, *J. Am. Chem. Soc.* **2002**, *124*, 2056; c) K. H. Thompson, C. Orvig, *Science* **2003**, *300*, 936; d) M. Querol, J. W. Chen, R. Weissleder, A. Bogdanov, Jr., *Org. Lett.* **2005**, *7*, 1719; e) A. Dirksen, S. Langereis, B. F. M. de Wall, M. H. P. van Genderen, T. M. Hackeng, E. M. Meijer, *Chem. Commun.* **2005**, 2811; f) C. Orvig, *Chem. Soc. Rev.* **2006**, *35*, 534.
- [18] C. M. Yang, J. Zhang, M. Lu, unpublished results.
- [19] a) S. L. C. Moors, M. Hellings, M. De Maeyer, Y. Engelborghs, A. Ceulemans, *Biophys. J.* **2006**, *91*, 816; b) K. J. Willis, W. Neugebauer, M. Sikorska, A. G. Szabo, *Biophys. J.* **1994**, *66*, 1623; c) C.-P. Pan, M. D. Barkley, *Biophys. J.* **2004**, *86*, 3828; d) G. Maglia, A. Jonckheer, M. De Maeyer, J.-M. Frere, Y. Engelborghs, *Protein Sci.* **2008**, *17*, 352.
- [20] a) B. J. Harvey, E. Bell, L. Brancalion, *J. Phys. Chem. B* **2007**, *111*, 2610; b) R. F. Chen, J. R. Knutson, H. Ziffer, D. Porter, *Biochemistry* **1991**, *30*, 5184; c) B. Liu, R. K. Thalji, P. D. Adams, F. R. Fronczek, M. L. McLaughlin, M. D. Barkley, *J. Am. Chem. Soc.* **2002**, *124*, 13329.
- [21] a) R. M. Roat-Malone, *Bioinorganic Chemistry*, Wiley, New York, **2002**, pp. 93–113; R. M. Roat-Malone, *Bioinorganic Chemistry*, Wiley, New York, **2002**, pp. 3–5; b) I. Tinoco, Jr., K. Sauer, J. C. Wang, J. D. Puglisi, *Physical Chemistry: Principles and Applications in Biological Sciences*, 4th ed., Prentice Hall, New Jersey **2002**, pp. 579–598; c) R. Sprangers, L. E. Kay, *Nat. Methods* **2007**, *4*, 697; d) V. Tugarinov, R. Sprangers, L. E. Kay, *J. Am. Chem. Soc.* **2007**, *129*, 1743.
- [22] C. Farès, I. Amata, T. Carlomagno, *J. Am. Chem. Soc.* **2007**, *129*, 15814.
- [23] a) Acidification of the apo-scaffolds with DCl also caused an upfield shift of the C4 of the Im ring, consistent with the binding of  $\text{Ca}^{2+}$  at the N3 position, but acidification by using DCl diminished the binding of metal to the scaffolds. b) For stable  $\text{Ca}^{2+}$  and  $\text{Mg}^{2+}$  binding with imidazole, see: Y. Unger, M. A. Taige, A. Ahrens, T. Strassner, *Inorg. Chim. Acta* **2007**, *360*, 3699; c) J. Reedijk, *Inorg. Chim. Acta* **1969**, *3*, 517; d) L. B. Cole, E. M. Holt, *J. Chem. Soc. Perkin Trans. 1* **1986**, 151.
- [24] a) Based on Alfred Werner's coordination theory, the structure of chiral EDTA- $\text{Ca}^{2+}$  complex was determined almost a century ago, see C. H. Eugster, *Chimia* **2008**, *62*, 75; b) J. P. Glusker, *Adv. Protein Chem.* **1991**, *42*, 1; c) W. Yang, A. L. Wilkins, S. Li, Y. Ye, J. J. Yang, *Biochemistry* **2005**, *44*, 8267.
- [25] P. Caravan, J. J. Ellison, T. J. McMurphy, R. B. Lauffer, *Chem. Rev.* **1999**, *99*, 2293.
- [26] M. J. Winter, *d-Block Chemistry*, Oxford University Press, New York, **2003**, pp. 33–34.
- [27] a) A. H. A. Clayton, W. H. Sawyer, *Biophys. J.* **1999**, *76*, 3235; b) M. P. Brown, C. Royer, *Curr. Opin. Biotechnol.* **1997**, *8*, 45; c) J. T. Vivian, P. R. Callis, *Biophys. J.* **2001**, *80*, 2093; d) P. D. Adams, Y. Chen, K. Ma, M. G. Zagorski, F. D. Sönnichsen, M. L. McLaughlin, M. D. Barkley, *J. Am. Chem. Soc.* **2002**, *124*, 9278.
- [28] a) R. L. Dunbrack, Jr., M. Karplus, *J. Mol. Biol.* **1993**, *230*, 543; b) J. Heringa, P. Argos, *Proteins Struct. Funct. Bioinf.* **1999**, *37*, 44.
- [29] a) M. J. McGregor, S. A. Islam, M. J. E. Sternberg, *J. Mol. Biol.* **1987**, *198*, 295; b) H. Schrauber, F. Eisenhaber, P. Argos, *J. Mol. Biol.* **1993**, *230*, 592; c) T. E. S. Dahms, K. J. Willis, A. G. Szabo, *J. Am. Chem. Soc.* **1995**, *117*, 2321.
- [30] a) E. V. Pletneva, A. T. Laederach, D. B. Fulton, N. M. Kostić, *J. Am. Chem. Soc.* **2001**, *123*, 6232; b) C. A. Hunter, C. M. R. Low, C. Rotger, J. G. Vinter, C. Zonta, *Proc. Natl. Acad. Sci. USA* **2002**, *99*, 4873; c) H. Suezawa, T. Hashimoto, K. Tsuchinaga, T. Yoshida, T. Yuzuri, K. Sakakibara, M. Hirota, M. Nishio, *J. Chem. Soc. Perkin Trans. 2* **2000**, 1243.
- [31] a) G. W. Gokel, *Chem. Commun.* **2002**, 1810; b) G. W. Gokel, *Chem. Commun.* **2003**, 2847.
- [32] Spartan'08 for Windows, Wavefunction, Irvine CA.
- [33] C. M. Yang, *Dalton Trans.*, in press.
- [34] a) K. S. Kim, J. Y. Lee, S. J. Lee, T.-K. Ha, D. H. Kim, *J. Am. Chem. Soc.* **1994**, *116*, 7399; b) S. Mecozzi, A. P. West, Jr., D. A. Dougherty, *J. Am. Chem. Soc.* **1996**, *118*, 2307; c) E. Cubero, F. J. Luque, M. Orozco, *Proc. Natl. Acad. Sci. USA* **1998**, *95*, 5976; d) S. Roelens, R. Torriti, *J. Am. Chem. Soc.* **1998**, *120*, 12443; e) S. Bartoli, S. Roelens, *J. Am. Chem. Soc.* **2002**, *124*, 8307.
- [35] a) M. Perutz, *Philos. Trans. R. Soc. London Ser. A* **1993**, *345*, 105; b) G. Tóth, R. F. Murphy, S. Lovas, *J. Am. Chem. Soc.* **2001**, *123*, 11782; c) G. Tóth, K. E. Kover, R. F. Murphy, S. Lovas, *J. Phys. Chem. B* **2004**, *108*, 9287; d) J. Kemmink, C. P. van Mierlo, R. M. Scheek, T. E. Creighton, *J. Mol. Biol.* **1993**, *230*, 312.
- [36] W. J. Hehre, *A Guide to Molecular Mechanics and Quantum Chemical Calculations*, Wavefunction, Irvine CA, 2003.

Received: November 17, 2009

Revised: April 23, 2010

Published online: July 28, 2010